Tibetan Plateau insights into >1100°C crustal melting in the Quaternary

Xiu-Zheng Zhang[1, 2] Qiang Wang[1, 2*] Derek Wyman[3] Andrew C. Kerr[4] Wei Dan[1, 2] Yue Qi[1, 2]

[1] *State Key Laboratory of Isotope Geochemistry, Guangzhou Institute of Geochemistry, Chinese Academy of Sciences, Guangzhou 510640, China*

[2] *CAS Center for Excellence in Deep Earth Science, Guangzhou, 510640, China*

[3] *School of Geosciences, The University of Sydney, NSW 2006, Australia*

[4] *School of Earth and Environmental Sciences, Cardiff University, Cardiff, CF10 3AT, UK*

* Qiang Wang, E-mail: wqiang@gig.ac.cn

ABSTRACT

Partial melting during high- to ultrahigh-temperature (UHT) metamorphism facilitates crustal differentiation, element transfer, and the evolution of topography in orogens, however the mechanisms that drive heating of Earth's crust remain controversial. In this contribution, we provide new evidence from ~2.3 Ma dacites in the Tibetan Plateau, the youngest known UHT metamorphic event. Our results show that these dacites were mainly generated by fluid-absent melting of metasedimentary rocks and minor mafic rocks at peak temperatures of 1100–1150 ℃ and pressures of 0.8–0.9 Gpa. The dacites represent mixtures of UHT melts and granulite residues and are geochemically similar to A-type granites with extremely high heat production values (5.33–5.99 μW m^{-3}). Compared with the geological and geophysical observations, numerical modelling indicates that the key factor determining the thermal evolution of Tibet is the thickness of the radioactive layer. Orogens dominated by rocks of felsic composition, like Tibet, could easily reach UHT conditions within a short period of time (20–40 million years) after crustal thickening by radioactive heating, without the need for an additional tectonic mechanism.

INTRODUCTION

Chemically evolved, silica-rich continental crust is a key feature of Earth (e.g., Rudnick, 1995). Partial melting during high-temperature metamorphism has played a dominant role in crustal differentiation, reworking, and element transfer throughout Earth history (Brown 2013; Cipar et al., 2020). Although, this substantial crustal melting plays a key role in the orogenic transition from linear mountain ranges to flat plateaus (Zhang et al., 2022), the primary mechanism that drives heating of Earth's crust remains enigmatic.

The identification of Ultra-high-temperature (UHT) metamorphism (>900°C with pressures of 0.7–1.3 Gpa; Harley & Motoyoshi, 2000; Brown, 2006) has extended our understanding of crustal evolution to very high thermal regimes. Hence, the UHT crustal record is generally accepted as the key to solving the mystery of Earth's crustal heating (Clark et al., 2011), although the driving tectonic mechanism remains controversial. Competing models have been proposed to account for extreme crustal temperatures, including the involvement of continental back-arcs (e.g., Brown 2006), long-lived mountain plateaus with high contents of heat-producing elements (Clark et al., 2011), post-thickening lithospheric extension (Cipar et al., 2020), and mantle plume impingement (Santosh et al., 2008).

Our understanding of the primary mechanism that generates UHT conditions is hindered by the uncertainties regarding tectonic setting. Furthermore, since most UHT records are from Neoarchean–Cambrian granulite rocks (e.g., Brown 2006), some key

information is commonly erased by long-term modification during their exhumation or later tectonism. However, in this paper we present new data (Figs. 1A-C) from the youngest known UHT melts and their residual granulite enclaves from the central Tibetan Plateau. This data provides an important information on the processes by which the continental crust of Tibet becomes extremely hot.

GEOLOGICAL SETTING

The Tibetan Plateau is the highest and largest orogenic plateau on Earth, and it has evolved from collision between India and Eurasia since *ca.* 60 Ma (e.g., Hu et al., 2015). The Qiangtang block (QB) lies in the central Tibetan Plateau and is divided into southern and northern Qiangtang (SQB and NQB) by the Paleo-Tethys Ocean suture zone (Fig. 1A) (Zhang et al., 2014). Cenozoic volcanic rocks occur widely in the QB and were erupted mainly in the Eocene–Oligocene (Wang et al., 2008, 2012). Geophysical data indicate that the present NQB probably has the highest thermal state of the entire plateau (Fig. 1A), and this is consistent with the occurrence of granulite xenoliths in the Dongyue Lake area (Hacker et al. 2000). The host lavas of these xenoliths have recently reclassified as dacites based on preliminary major- and trace-element analyses (Wang et al., 2016). The present study focuses on these dacites and enclaves from the Dongyue Lake area of the NQB, and confirms that they are UHT melts containing granulite residues.

PETROGRAPHY

74 The NQB dacites contain phenocrysts of plagioclase (Pl), K-feldspar (Ksp), and quartz
75 (Qtz) in a cryptocrystalline–glassy groundmass. They record 10–20 vol.% entrainment
76 of restite from the source, including phenocryst-like peritectic minerals (Figs. S1A-E)
77 and millimeter-scale granulite enclaves (Fig. S1F). The restites have consistent
78 compositions that are similar to those of typical UHT pelitic granulites, including high-
79 F phlogopite (Phl; F = 4.4–5.5 wt.%), aluminous orthopyroxene (Opx_{Al}; Al_2O_3 = 7.2–
80 9.0 wt.%), spinel (Sp), Ksp, ilmenite (Ilm), and minor titanomagnetite (Tim) (Table S1).
81 They also contain minor high-F pargasite (Prg; F = ~1.8 wt.%; Table S1),
82 orthopyroxene (Opx) and clinopyroxene (Cpx), minerals typical of UHT mafic
83 granulites (e.g., Tsunogae et al., 2003). Although most high-F Phl and Prg in the dacites
84 are euhedral–subhedral and almost indistinguishable from phenocrysts in texture, their
85 compositions are similar to those of crystals in the UHT granulite enclaves of this study
86 (Table S1) and those worldwide (e.g., the Napier Complex in East Antarctica;
87 Motoyoshi and Hensen, 2001; Tsunogae et al., 2003). This confirms that they are
88 entrained peritectic minerals of metamorphic origin.
89
90 A granulite enclave from sample 5123-2 is heterogeneous at the millimeter scale and
91 can be divided into melanocratic domains of Opx_{Al} + Sp + Ksp + Ilm and leucocratic
92 domains of Pl + Ksp + Phl ± Qtz (Figs. 2 and S1). Phl occurs locally as a relict mineral
93 which has partially broken down to Opx_{Al} + Sp ± Ilm (Figs. S1G, H). Opx_{Al} occurs in
94 aggregates and has a maximum Al_2O_3 content of 8.3–9.0 wt.%. Ksp has X_{an} (Ca/ (Ca +
95 Na + K)) values of 0.03–0.05. A P–T pseudosection was calculated and contoured with

isopleths of $Al^{IV}(Opx_{Al})$ and $X_{An}(Ksp)$ for relevant assemblages (Fig. 2A). Al in Opx_{Al} is widely used as a geothermometer for UHT metamorphism due to its low diffusion rate (Kelsey, 2008). The observed Opx_{Al} + Sp + Ilm + Ksp assemblage (Figs. 2B, C), which has the highest Al^{IV} value of 0.20–0.21, is predicted to be stable at 1100°C–1150°C and pressures of 0.8–0.9 Gpa (Fig. 2A), representing peak conditions. Some Opx_{Al} which occurs as individual minerals in the matrix with relatively low Al^{IV} values of 0.17–0.20 (Table S1), is a prograde metamorphic mineral. The observed minerals and enclaves are thus residual materials formed during a series of UHT metamorphic reactions below or at peak conditions.

GEOCHRONOLOGY AND ISOTOPIC COMPOSITIONS

Dacite samples 5123-2 and 5124-2 yielded weighted-mean whole-rock $^{40}Ar/^{39}Ar$ ages of 2.95 ± 0.73 Ma and 3.16 ± 0.59 Ma, respectively, and sample 5126-1 yielded a weighted-mean phlogopite $^{40}Ar/^{39}Ar$ age of 2.20 ± 0.15 Ma (Figs. 1C, S2; Table S2). In addition, three dacite samples (5123-2, 5126-1, and 5133) were selected for zircon U–Pb dating by secondary-ion mass spectrometry. Most of the zircon grains show concentric oscillatory zoning in cathodoluminescence images (Fig. S2), and have high Th/U ratios (0.62–3.54), indicating a magmatic origin (Hoskin and Schaltegger, 2000). Results of 37 analyses were identical within analytical uncertainty, yielding a weighted-mean age of 2.29 ± 0.08 Ma (Fig. 1B; Table S3). This is interpreted as the crystallization age of these dacites, consistent with the zircon U–Pb age range of the three individual samples of 2.36 ± 0.11 Ma to 2.23 ± 0.10 Ma (Fig. S2).

The dacites have near-identical Pb isotopic compositions ($^{206}Pb/^{204}Pb$, 18.80–18.89; $^{207}Pb/^{204}Pb$, 15.73–15.80; $^{208}Pb/^{204}Pb$, 39.29–39.47; Table S4), similar to those of marine sediments and granulite xenoliths in QB Cenozoic volcanic rocks (Figs. 3A, B). *In situ* zircon Hf–O isotopic analyses of three dacite samples yielded variable $\varepsilon_{Hf}(t)$ values of +0.6 to –25.9 and $\delta^{18}O$ values of 6.1–8.0 (Table S5), broadly similar to those of S-type granites (Fig. 3C).

DISCUSSION

Insights from the youngest known example of UHT crustal reworking

In contrast to the prolonged cooling of HT–UHT granulite terrains (e.g., Wang et al., 2020), the cooling of granulite enclaves in volcanic rocks may be rapid (minutes to months; Cesare, 2008). It follows that the phlogopite $^{40}Ar/^{39}Ar$ cooling age of *ca.* 2.2 Ma should reflect (or be close to) the timing of UHT metamorphism, which is consistent with the metamorphic ages (~2.5–3.4 Ma) obtained in previous study (Hacker et al., 2000). Combined with the mineralogical observations and the same metamorphic and magmatic ages, the dacites and their entrainment of granulite residues are products of the same UHT metamorphism/partial melting event beneath the NQB.

The dacites thus represent the youngest (2.3 Ma) and hottest (>1100°C) crustal melting recorded to date, providing new insights into crustal reworking under extreme conditions: (1) This study provides a clear modern tectonic setting, in a collisional

orogen with thickened crust, in which UHT conditions can be generated. (2) Mineralogical evidence indicates that UHT crustal felsic magma is a mixture of melt with a peritectic assemblage of entrained and residual granulite enclaves. The residues are mainly composed of UHT pelitic granulites and a small amount of mafic granulites (Fig. S1), indicating that the NQB dacites were generated by partial melting of metasedimentary rocks and minor mafic rocks. This is consistent with their zircon Hf–O and whole-rock Pb isotopic compositions (Figs. 3A-C). (3) The substitution of F for OH in the nominally hydrous minerals (Phl and Prg) of the present study implies that UHT partial melting occurs under extreme H_2O-poor conditions. (4) The UHT crustal magmas are geochemically characterized by both high 10000Ga/Al ratios and zircon saturation temperatures (946–973 ºC) in conjunction low Sr/Y values (Fig. S3) (Wang et al., 2016), similar to typical "A-type" granites. They also have extremely high heat-production values of 5.33–5.99 μW m^{-3} (Fig. 3D). Hence UHT partial melting and melt migration may thus enhance the transfer of radioactive elements from the deep crust to the upper crust.

How does orogenic crust get extremely hot?

UHT metamorphism is not usually associated with mantle-derived magmas (e.g., Clark et al., 2011). This is consistent with the scarcity of Quaternary mafic–ultramafic magmatism in the NQB. In a large collisional orogen, radioactive heat production in thickening crust (Clark et al., 2011) in combination with thinning lithosphere (Cipar et al., 2020; Wang et al., 2020) may play a key role in generating UHT conditions.

The Tibetan Plateau is a young active orogen and most of its evolutionary controls are known or well defined. Geophysical data indicate that the NQB has thick (~70 km) continental crust and a thin (~150 km) lithosphere (Gao et al., 2013; Tunini et al., 2016). The occurrence of Eocene (47–38 Ma) eclogitic crust-derived adakitic rocks indicates that the NQB crust has been thickened since *ca.* 47 Ma (Wang et al., 2008), likely reaching its near-present thickness during the Eocene (e.g., Wang et al., 2014). Therefore, the NQB has attained UHT conditions (>1100°C) relatively rapidly over a period of < 45 million years (Myr) after crustal thickening, much shorter than previous estimates of ~120 Myr (Clark et al., 2011). Furthermore, low erosion rates of <0.05 mm yr^{-1} since *ca.* 45 Ma have been estimated for central Tibet (Rohrmann et al., 2012). Based on these considerations, we used a 1-dimensional thermal model to reproduce the development of UHT conditions in the NQB according to two alternative end-member crustal models (Figs. 4A, B).

The "classic" Alps-type crustal model involves a 20-km-thick radioactive felsic upper layer and a 15-km-thick lower non-radioactive mafic layer, which doubles in thickness at 47 Ma by homogenous deformation (Fig. 4A). To replicate the extreme temperature of the NQB requires an extremely high radioactive heat production (>4.0 μW m^{-3}) (Fig. 4C). The calculated heat-production of Devonian–Eocene felsic rocks from NQB is 1.66–2.96 μW m^{-3} (Fig. 3D), averaging 2.54 μW m^{-3} (Table S6), much lower than theoretical requirements. Hence this model does not fit with geological observations in

184 Tibet.

185

186 The Tibet-type crustal model (Fig. 4B) indicates that the NQB could have a more silica-
187 rich lower crust, corresponding to a much thicker (≥ 60 km) radioactive layer in the
188 thickened crust. In this model the UHT conditions of NQB can be reproduced with a
189 normal heat production of ~2.5 μW m^{-3} (Fig. 4D). In addition, the thermal evolution of
190 the NQB crust based on this model is consistent with the metamorphic evolution of the
191 NQB as inferred from crustal xenoliths (Fig. 4E) (Zhang et al., 2022). Furthermore,
192 recent geophysical data indicate that the thick Tibetan crust lacks a mafic lower layer
193 and is predominantly felsic in composition (Wang et al., 2021). Therefore, a more felsic
194 and radioactive lower crust is likely to be a primary requirement for the development
195 of UHT conditions during continental collision.

196

197 The composition of the lower crust remains controversial but recent studies demonstrate
198 that at least some of lower crust need not be mafic and the bulk continental crust may
199 be more silica rich than generally thought (Hacker et al., 2011; Wang et al., 2021).
200 During sediment subduction, subduction erosion, and continent subduction, the original
201 lower crust of the upper plate could be reworked into more felsic crust by relamination
202 (Hacker et al., 2011). Qiangtang and other Tibetan blocks have undergone long-term
203 subduction of the oceanic lithosphere and multi-stage continental collision because of
204 subduction and closure of the intervening Tethyan oceans (e.g., Zhang et al., 2014).
205 Therefore, felsic rocks could form much of the Tibetan lower crust, which is consistent

with geophysical observations (Wang et al., 2021) and our numerical modelling (Fig. 4).

Modelling with both a thin lithosphere thickness of 150 km and normal lithosphere (190 km) was undertaken to assess the effect of lithospheric thinning on thermal evolution (Tunini et al., 2016; Molnar et al., 1993). The results of this modelling are shown in Fig. 4C, D and significantly, the difference in heating between the two cases was not as marked as expected, indicating that lithospheric thinning has very little influence.

IMPLICATIONS

Insights this young UHT terrane in the Tibetan Plateau confirm that the orogen is an important tectonic setting in which UHT conditions can develop. If an orogen has a Tibet-type crust with predominantly felsic rocks, then its entire middle–lower crust can reach UHT conditions within 20–40 Myr after crustal thickening via radioactive heating (Fig. 4E). These high temperatures can develop without the need for anomalously high heat production or lithospheric thinning. HT-UHT conditions will trigger substantial partial melting, crustal weakening, and crustal flow, leading to the transformation of linear mountain ranges to flat plateaus (Zhang et al., 2022). In contrast, orogens with Alps-type crust (more mafic lower crust) have difficulty attaining high temperatures unless prolonged (>120 Myr) radioactive heating occurs at very low erosion rates (Clark et al., 2011). This observation explains the varying thermal state, metamorphism and topographic features in different orogens throughout Earth history.

ACKNOWLEDGMENTS

We acknowledge editor Marc Norman, Haijun Xu, and an anonymous reviewer for constructive suggestions. This study was jointly supported by the Second Tibetan Plateau Scientific Expedition and Research program (STEP) (Grant No. 2019QZKK0702) and the National Natural Science Foundation of China (Nos. 41872065, 42021002 and 91855215). This is contribution No. IS–XXXX from GIGCAS.

FIGURE CAPTIONS

Figure 1. (A) Geological sketch map of Tibet showing major blocks, Cenozoic magmatic rocks, and geothermal state (i.e., depth of the 1250°C isotherms; Deng et al., 2016). NQB, northern Qiangtang Block; SQB, southern Qiangtang Block; IYZS, Indus–Yarlung Zangbo Suture; BNS, Bangong–Nujiang Suture; JS, Jinsha Suture; LSS, Longmu Co-Shuanghu Suture; AKMS, Anymaqen–Kunlun–Muztagh Suture. (B) Zircon U–Pb data of dacites. (C) $^{40}Ar/^{39}Ar$ age spectra of phlogopite.

Figure 2. (A) P–T pseudosection for the UHT granulite. (B) Photomicrograph (plane-polarized light) of UHT granulite and host dacite and (C) back-scattered electron image. L, melt; Opx_{Al}, aluminous orthopyroxene; Sp, spinel; Ksp, K-feldspar; Grt, garnet; Sa, sapphirine; Ilm, ilmenite; Pl, plagioclase; Cd, cordierite.

Figure. 3 (A) $^{206}Pb/^{204}Pb$–$^{208}Pb/^{204}Pb$ diagram. (B) $^{206}Pb/^{204}Pb$–$^{207}Pb/^{204}Pb$ diagram. (C) εHf(t)–$\delta^{18}O$ diagram (t = 2.3 Ma). (D) The calculated heat-production of Devonian–Quaternary felsic rocks from NQB (Table S6). Data of granulite xenoliths in the QB are after Lai and Qin (2008). The field for Hf–O isotopic compositions of S-type granites is after Kemp et al. (2007). The mean value of heat production in global granitic crust is from Artemieva et al. (2017). NHRL: Northern Hemisphere Reference Line. EM1 and EM2: enriched mantle end-members (Zindler & Hart, 1986).

Figure. 4 1D thermal model of UHT conditions in the QB. (A) Alps-type and (B) Tibet-type crustal models. (C) Modelled geothermal gradient at 2.3 Ma based on Alps-type crustal model, with varying rates of heat production (A_{rad}) for felsic crust. (D) Modelled geothermal gradient at 2.3 Ma based on a normal heat production of 2.5 μW m^{-3}, with varying thickness of felsic crust. (E) P–T evolution of the QB based on Tibet-type crustal model from initial crustal thickening at 47 Ma to the present. Modelling generally follows the code of Clark et al. (2011). A latent heat of melting (320 kJ kg^{-1}) was included in all modelling.

References

Artemieva, I.M., Thybo, H., Jakobsen, K., Sørensen, N.K., Nielsen, L.S.K., 2017, Heat production in granitic rocks: Global analysis based on a new data compilation GRANITE2017: Earth-Science Reviews, v. 172, p. 1–26

Brown, M., 2006, Duality of thermal regimes is the distinctive characteristic of plate

tectonics since the Neoarchaean: Geology, v. 34, p. 961–964.

Brown, M., 2013, Granite: from genesis to emplacement: Geological Society of America Bulletin, v.125, no. 7–8, p. 1079–1113.

Cesare, B., 2008, Crustal melting: working with enclaves. In: Sawyer, E. W. & Brown, M. (eds) Working with Migmatites. Mineralogical Association of Canada, Short Course, v. 38, p. 37–55.

Cipar, J.H., Garber, J.M., Kylander-Clark, A.R., Smye, A.J., 2020, Active crustal differentiation beneath the Rio Grande Rift: Nature Geoscience, v. 13, p. 758–763.

Clark, C., Fitzsimons, I. C. W., Healy, D. & Harley, S. L., 2011, How does the continental crust get really hot: Elements, v. 7, p. 235–240.

Deng, Y., and Tesauro, M., 2016, Lithospheric strength variations in Mainland China: Tectonic implications: Tectonics, v. 35, p. 2313–2333.

Gao, R., Chen, C., Lu, Z. W., Brown, L. D., Xiong, X. S., Li, W. H., & Deng, G., 2013, New constraints on crustal structure and Moho topography in Central Tibet revealed by SinoProbe deep seismic reflection profiling: Tectonophysics, v. 606, p. 160–170.

Hacker B.R, Kelemen PB, Behn M.D., 2011, Differentiation of the continental crust by relamination: Earth and Planetary Science Letters, v. 307, p. 501–16.

Hacker, B.R., Gnos, E., Ratschbacher, L., Grove, M., McWilliams, M., Sobolev, S.V., Wan, J. and Wu, Z.H., 2000, Hot and dry deep crustal xenoliths from Tibet: Science, v. 287, p. 2463–2466.

Harley, S.L. & Motoyoshi, Y., 2000, Al zoning in orthopyroxene in a sapphirine

quartzite: evidence for >1120 ℃ UHT metamorphism in the Napier complex, Antarctica, and implications for the entropy of sapphirine: Contributions to Mineralogy and Petrology, v. 138, p. 293–307.

Hu, X., Garzanti, E., Moore, T., Raffi, I., 2015, Direct stratigraphic dating of India-Asia collision onset at the Selandian (middle Paleocene, 59 ± 1 Ma): Geology, v. 43, no. 10, p. 859–862.

Hoskin, P.W.O., Black, L.P., 2000, Metamorphic zircon formation by solid-state recrystallization of protolith igneous zircon: Journal of Metamorphic Geology, v. 18, no. 4, p. 423–439.

Kelsey, D.E., 2008, On ultrahigh-temperature crustal metamorphism: Gondwana Research, v. 13, p.1–29.

Kemp, A.I.S., Hawkesworth, C. J., Foster, G.L., Paterson, B.A., Woodhead, J.D., Hergt, J.M., Gray, C.M., and Whitehouse, M.J., 2007, Magmatic and Crustal Differentiation History of Granitic Rocks from Hf-O Isotopes in Zircon: Science, v. 315, p. 980–983.

Lai, S.C., and Qin, J.F., 2008, Petrology and geochemistry of the granulite xenoliths from Cenozoic Qiangtang volcanic field：Implication for the nature of the lower crust in the northern Tibetan plateau an d the genesis of Cenozoic volcanic rocks: Acta Petrologica Sinica, v. 24, p. 325–336.

Long, X., Wilde, S.A., Wang, Q., Yuan, C., Wang, X.C., Li, J., Jiang, Z., Dan, W., 2015, Partial melting of thickened continental crust in central Tibet: Evidence from geochemistry and geochronology of Eocene adakitic rhyolites in the northern

316 Qiangtang Terrane: Earth and Planetary Science Letters, v. 414, p. 30–44.
317 Molnar, P., England, P., & Martinod, J., 1993, Mantle dynamics, the uplift of the Tibetan
318 plateau, and the Indian monsoon: Review of Geophysics, v. 31, p. 357–396.
319 Motoyoshi, Y., Hensen, B.J., 2001, F-rich phlogopite stability in ultra-high temperature
320 metapelites from the Napier Complex, East Antarctica: American Mineralogist, v.
321 86, p. 1404–1413.
322 Rohrmann, A., Kapp, P., Carrapa, B., Reiners, P.W., Guynn, J., Ding, L., and Heizler,
323 M., 2012, Thermochronologic evidence for plateau formation in central Tibet by
324 45 Ma: Geology, v. 40, p. 187–190.
325 Rudnick, R.L., 1995, Making continental crust. Nature, v. 378, p. 571–578.
326 Santosh, M., Tsunogae, T., Ohyama, H., Sato, K., Li, J.H. & Liu, S.J., 2008, Carbonic
327 metamorphism at ultrahigh temperatures: Evidence from North China Craton:
328 Earth and Planetary Science Letters, v. 266, p. 149–165.
329 Tsunogae, T., Osanai, Y., Owada, M., Toyoshima, T., Hokada, T., Crowe, W.A., 2003,
330 High fluorine pargasites in ultrahigh temperature granulites from Tonagh Island in
331 the Archean Napier Complex, East Antarctica: Lithos, v. 70, p. 21–38.
332 Tunini, L., Jiménez-Munt, I., Fernandez, M., Vergés, J., Villaseñor, A., Melchiorre, M.,
333 and Afonso, J.C., 2016, Geophysical petrological model of the crust and upper
334 mantle in the India-Eurasia collision zone: Tectonics, v. 35, p.1642–1669.
335 Valley, J.W., Kinny, P.D., Schulze, D.J., Spicuzza, M.J., 1998, Zircon megacrysts from
336 kimberlite: oxygen isotope variability among mantle melts: Contributions to
337 Mineralogy and Petrology, v. 133, p. 1–11.

Wang B., Wei C.J., Tian W., Fu B., 2020, UHT metamorphism peaking above 1100 °C with slow cooling: insights from pelitic granulites in the Jining complex, North China Craton: Journal of Petrology, v. 61, no. 6, p. egaa070.

Wang, Q., Wyman, D.A., Xu, J., Dong, Y., Vasconcelos, P.M., Pearson, N., Wan, Y., Dong, H., Li, C., Yu, Y., Zhu, T., Feng, X., Zhang, Q., Zi, F. Chu, Z., 2008, Eocene melting of subducting continental crust and early uplifting of central Tibet: Evidence from central–western Qiangtang high-K calc-alkaline andesites, dacites and rhyolites: Earth and Planetary Science Letters, v. 272, p. 158–171.

Wang, Q., Chung, S.L., Li, X.H., Wyman, D., Li, Z.X., Sun, W.D., Qiu, H.N., Liu, Y.S., Zhu, Y.T., 2012, Crustal melting and flow beneath northern Tibet: Evidence from Mid-Miocene to Quaternary strongly peraluminous rhyolites in southern Kunlun Range: Journal of Petrology, v. 53, no. 12, p. 2523–2566.

Wang, Q., Hawkesworth, C.J., Wymane, D., Chung, S. L., Wug, F.Y., Li, X.H., Li, Z. X., Gou, G.N., Zhang, Z.X., Tang, G.J., Dan, W., Ma, L., Dong, Y.H., 2016, Pliocene–Quaternary crustal melting in central and northern Tibet with new insights into crustal flow: Nature Communications, doi: 10.1038/ncomms11888.

Wang, C., Dai, J., Zhao, X., Li, Y., Graham, S.A., He, D., Ran, B., Meng, J., 2014, Outward growth of the Tibetan Plateau during the Cenozoic: a review: Tectonophysics, v. 621, p. 1–43.

Wang, G., Thybo, H. & Artemieva, I. M., 2021, No mafic layer in 80 km thick Tibetan crust. Nature Communications, v. 12, p. 1069.

Zeng, Y., Ducea, M.N., Xu, J., Chen, J., Dong, Y.H., 2020, Negligible surface uplift

following foundering of thickened central Tibetan lower crust: Geology, v. 49, p. 45–50.

Zhang, X.Z., Dong, Y.S., Li, C., Deng, M.R., Zhang, L., Xu, W., 2014, Silurian high–pressure granulites from Central Qiangtang, Tibet: Constraints on early Paleozoic collision along the northeastern margin of Gondwana: Earth and Planetary Science Letters, v. 405, p. 39–51.

Zhang, X.Z., Wang, Q., Wyman, D., Ou, Q., Qi, Y., Gou, G.N., Dan, W., Yang, Y.N., 2022, Tibetan Plateau growth linked to crustal thermal transitions since the Miocene: Geology, v.50, no. 5, p. 610–614.

Zindler, A., Hart, S., 1986, Chemical geodynamics: Annual Review of Earth and Planetary Sciences, v. 14, p. 493–571.

Figure 1

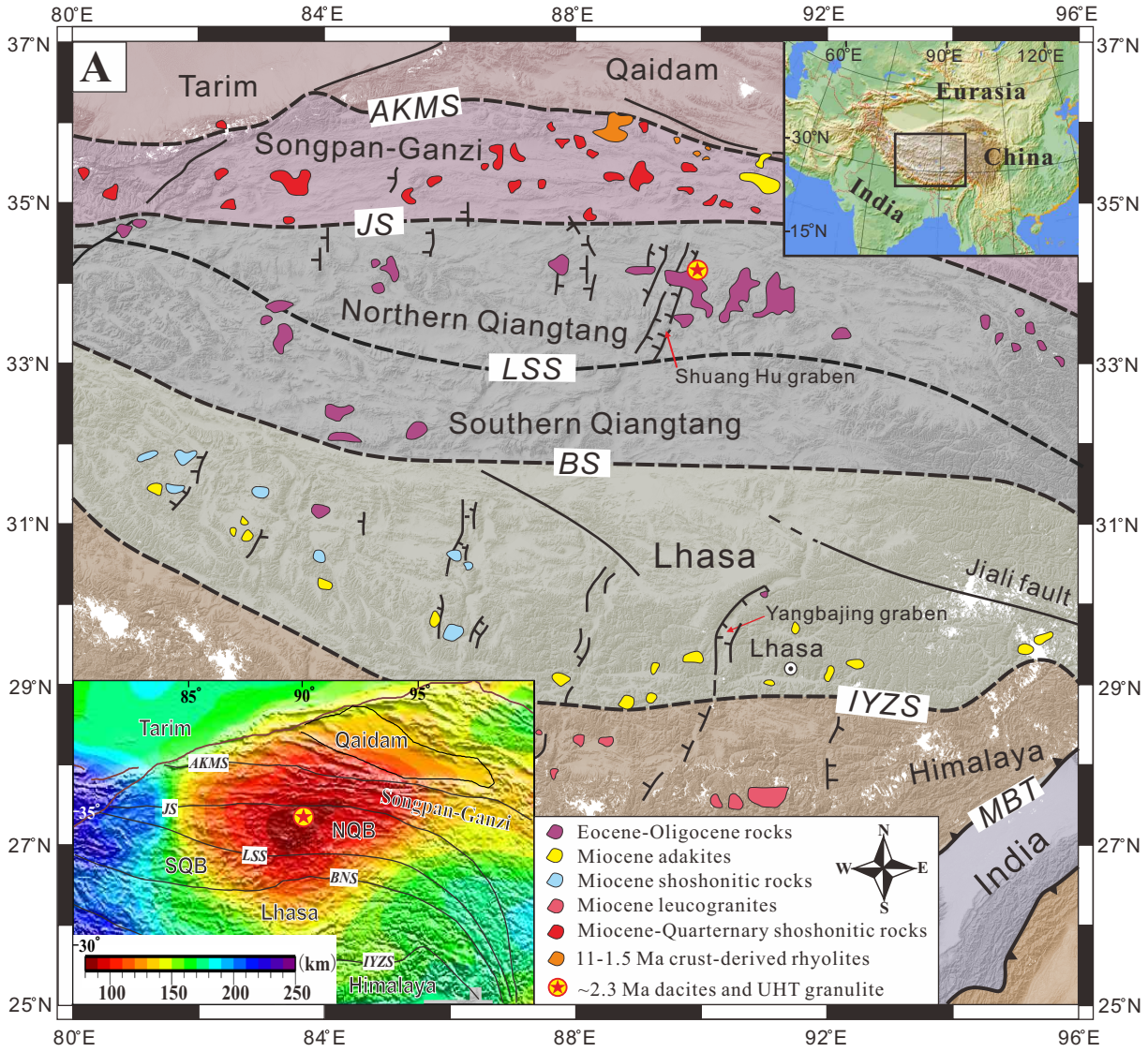
A
Tarim
Qaidam
AKMS
Songpan-Ganzi
JS
Northern Qiangtang
LSS
Shuang Hu graben
Southern Qiangtang
BS
Lhasa
Jiali fault
Yangbajing graben
Lhasa
IYZS
Himalaya
MBT
India
Eurasia
China
India
NQB
SQB
BNS
(km)
Eocene-Oligocene rocks
Miocene adakites
Miocene shoshonitic rocks
Miocene leucogranites
Miocene-Quarternary shoshonitic rocks
11-1.5 Ma crust-derived rhyolites
~2.3 Ma dacites and UHT granulite

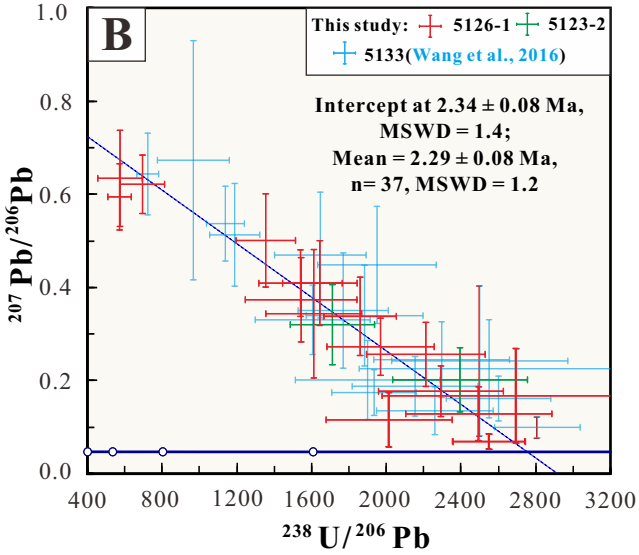
B
This study: 5126-1 5123-2
5133(Wang et al., 2016)
Intercept at 2.34 ± 0.08 Ma,
MSWD = 1.4;
Mean = 2.29 ± 0.08 Ma,
n= 37, MSWD = 1.2
207 Pb/206 Pb
238 U/206 Pb

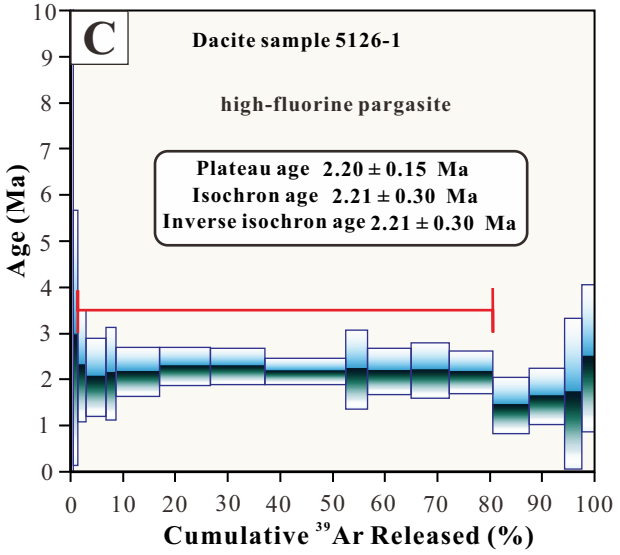
C
Dacite sample 5126-1
high-fluorine pargasite
Plateau age 2.20 ± 0.15 Ma
Isochron age 2.21 ± 0.30 Ma
Inverse isochron age 2.21 ± 0.30 Ma
Age (Ma)
Cumulative 39Ar Released (%)

Figure 2

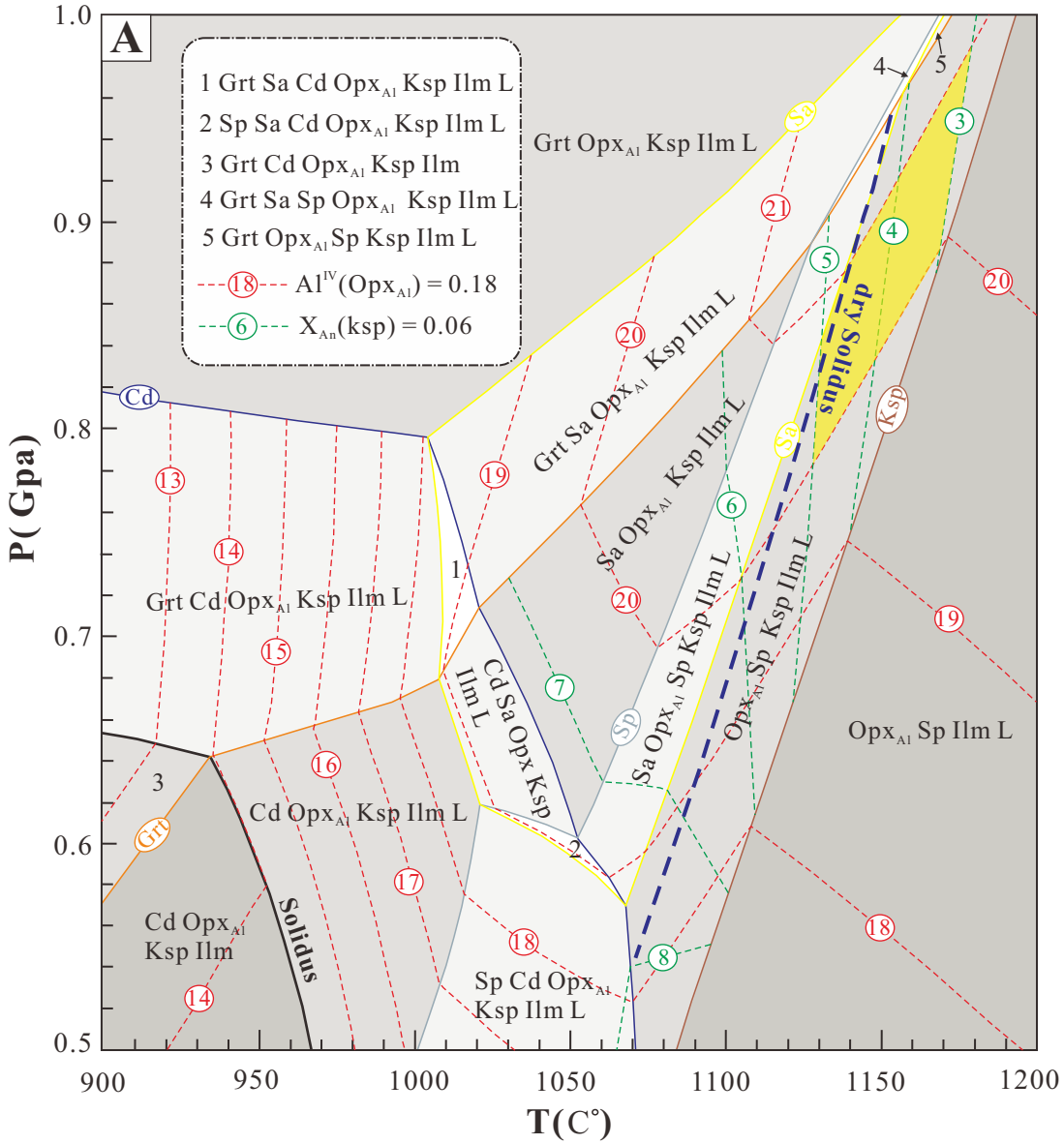
A
1 Grt Sa Cd Opx$_{Al}$ Ksp Ilm L
2 Sp Sa Cd Opx$_{Al}$ Ksp Ilm L
3 Grt Cd Opx$_{Al}$ Ksp Ilm
4 Grt Sa Sp Opx$_{Al}$ Ksp Ilm L
5 Grt Opx$_{Al}$ Sp Ksp Ilm L
Al^{IV}(Opx$_{Al}$) = 0.18
X$_{An}$(ksp) = 0.06
Grt Opx$_{Al}$ Ksp Ilm L
Grt Sa Opx$_{Al}$ Ksp Ilm L
Sa Opx$_{Al}$ Ksp Ilm L
Sa Opx$_{Al}$ Sp Ksp Ilm L
Opx$_{Al}$ Sp Ksp Ilm L
Opx$_{Al}$ Sp Ilm L
Grt Cd Opx$_{Al}$ Ksp Ilm L
Cd Sa Opx Ksp Ilm L
Cd Opx$_{Al}$ Ksp Ilm L
Cd Opx$_{Al}$ Ksp Ilm
Sp Cd Opx$_{Al}$ Ksp Ilm L
dry Solidus
Solidus
Cd
Grt
Sa
Sp
Ksp
P(Gpa)
T(C°)
1.0
0.9
0.8
0.7
0.6
0.5
900
950
1000
1050
1100
1150
1200

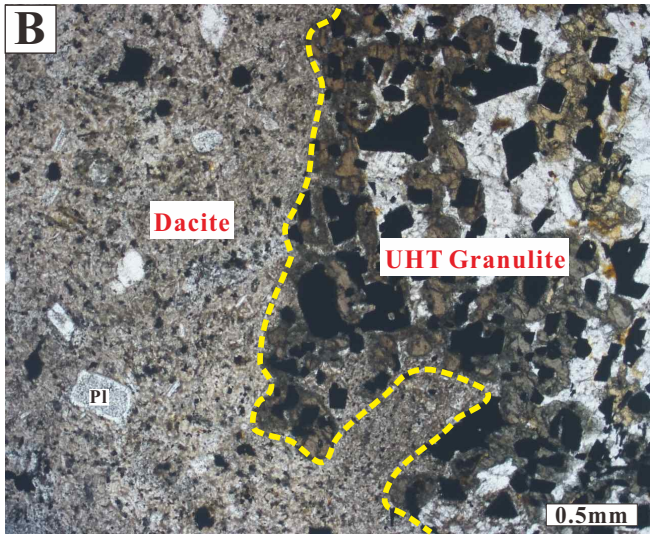
B
Dacite
UHT Granulite
Pl
0.5mm

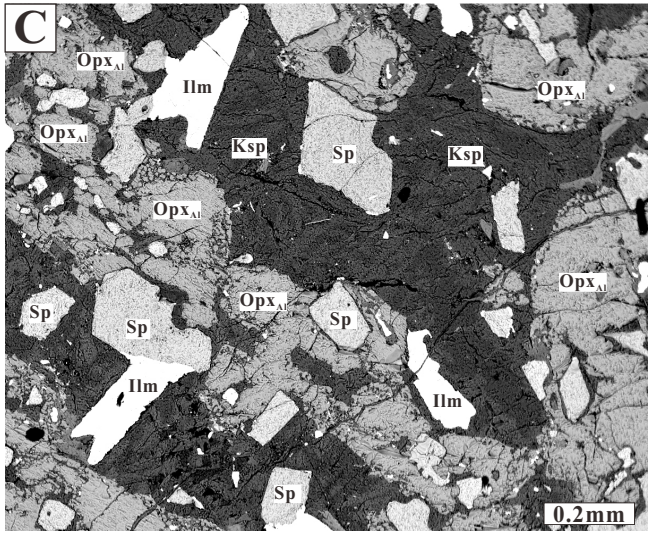
C
Opx$_{Al}$
Ilm
Ksp
Sp
0.2mm

Figure 3

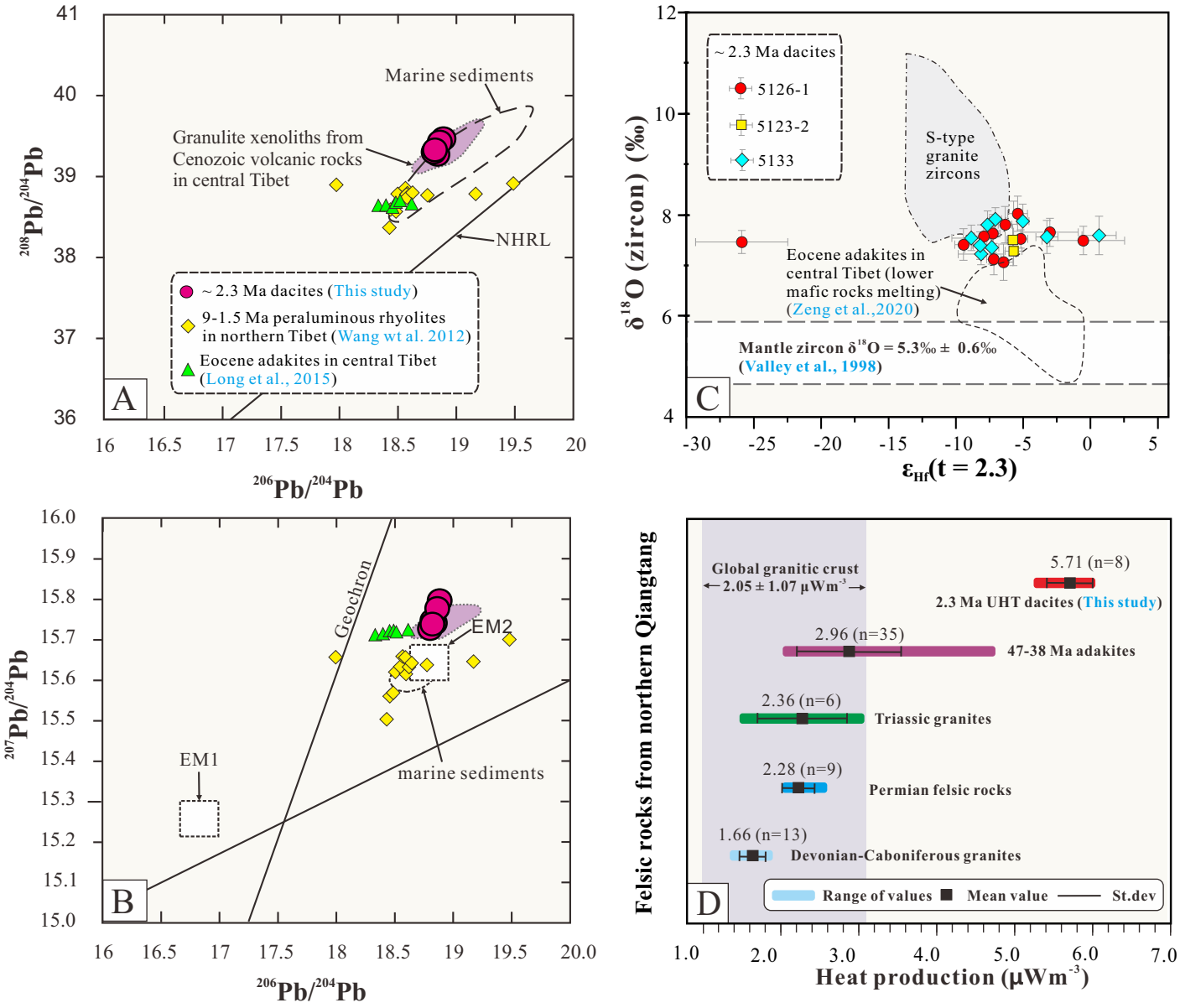
A
Marine sediments
Granulite xenoliths from Cenozoic volcanic rocks in central Tibet
NHRL
~ 2.3 Ma dacites (This study)
9-1.5 Ma peraluminous rhyolites in northern Tibet (Wang wt al. 2012)
Eocene adakites in central Tibet (Long et al., 2015)
$^{208}Pb/^{204}Pb$
$^{206}Pb/^{204}Pb$
B
Geochron
EM2
EM1
marine sediments
$^{207}Pb/^{204}Pb$
$^{206}Pb/^{204}Pb$
C
~ 2.3 Ma dacites
5126-1
5123-2
5133
S-type granite zircons
Eocene adakites in central Tibet (lower mafic rocks melting) (Zeng et al.,2020)
Mantle zircon $\delta^{18}O = 5.3‰ \pm 0.6‰$ (Valley et al., 1998)
$\delta^{18}O$ (zircon) (‰)
$\varepsilon_{Hf}(t = 2.3)$
D
Global granitic crust
$2.05 \pm 1.07\ \mu Wm^{-3}$
5.71 (n=8)
2.3 Ma UHT dacites (This study)
2.96 (n=35)
47-38 Ma adakites
2.36 (n=6)
Triassic granites
2.28 (n=9)
Permian felsic rocks
1.66 (n=13)
Devonian-Caboniferous granites
Range of values
Mean value
St.dev
Felsic rocks from northern Qiangtang
Heat production (μWm^{-3})

Figure 4

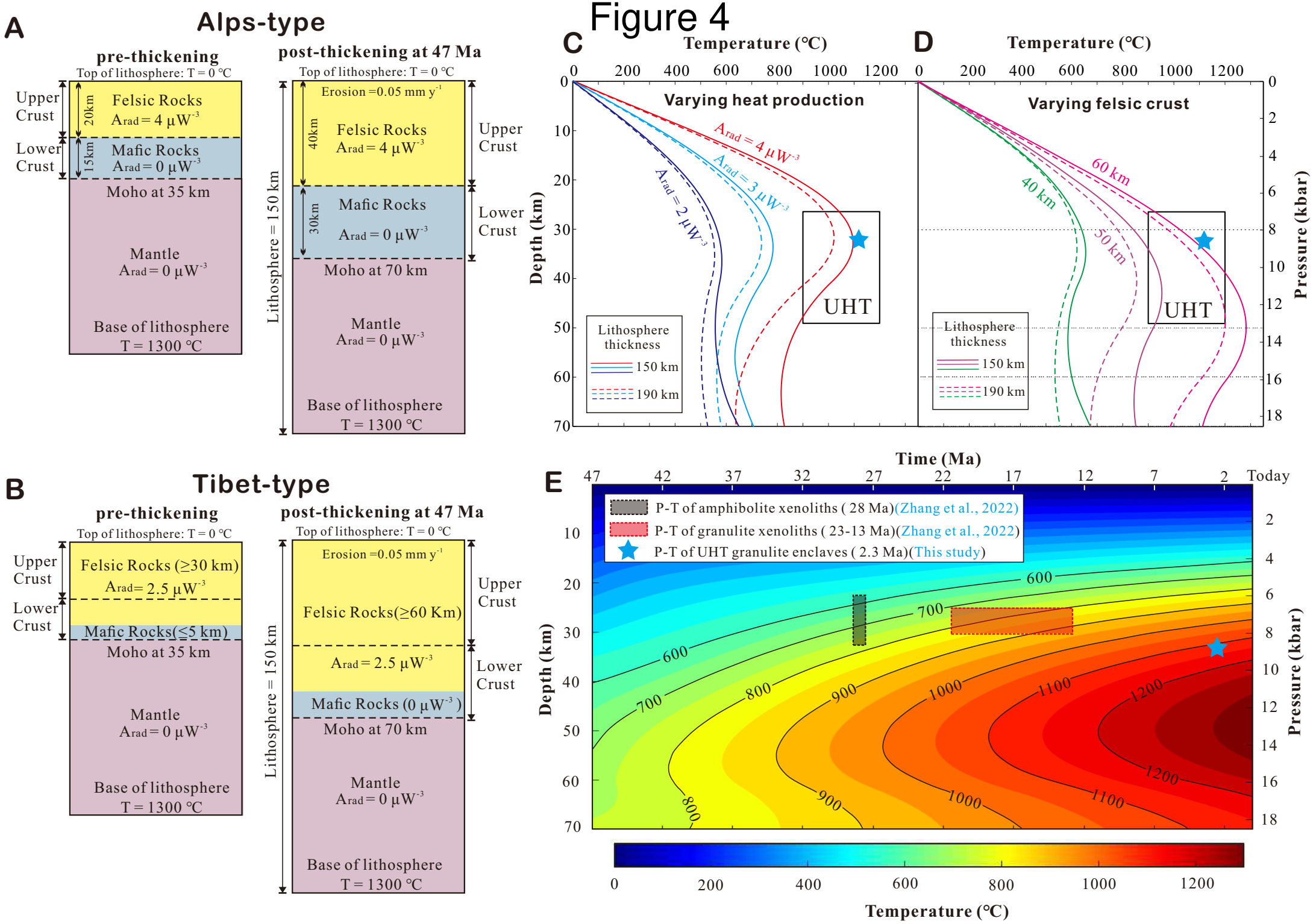
A
Alps-type
pre-thickening
Top of lithosphere: T = 0 °C
Upper Crust
Lower Crust
20km
15km
Felsic Rocks
Arad = 4 μW-3
Mafic Rocks
Arad = 0 μW-3
Moho at 35 km
Mantle
Arad = 0 μW-3
Base of lithosphere
T = 1300 °C
post-thickening at 47 Ma
Top of lithosphere: T = 0 °C
Erosion =0.05 mm y-1
40km
30km
Lithosphere = 150 km
Felsic Rocks
Arad = 4 μW-3
Mafic Rocks
Arad = 0 μW-3
Moho at 70 km
Mantle
Arad = 0 μW-3
Base of lithosphere
T = 1300 °C
B
Tibet-type
pre-thickening
Top of lithosphere: T = 0 °C
Felsic Rocks (≥30 km)
Arad= 2.5 μW-3
Mafic Rocks(≤5 km)
Moho at 35 km
Mantle
Arad = 0 μW-3
Base of lithosphere
T = 1300 °C
post-thickening at 47 Ma
Top of lithosphere: T = 0 °C
Erosion =0.05 mm y-1
Felsic Rocks(≥60 Km)
Arad = 2.5 μW-3
Mafic Rocks (0 μW-3)
Moho at 70 km
Mantle
Arad = 0 μW-3
Base of lithosphere
T = 1300 °C
C
Temperature (°C)
Varying heat production
Arad = 4 μW-3
Arad = 3 μW-3
Arad = 2 μW-3
UHT
Lithosphere thickness
150 km
190 km
Depth (km)
D
Temperature (°C)
Varying felsic crust
60 km
40 km
50 km
UHT
Lithosphere thickness
150 km
190 km
Pressure (kbar)
E
Time (Ma)
Today
P-T of amphibolite xenoliths (28 Ma)(Zhang et al., 2022)
P-T of granulite xenoliths (23-13 Ma)(Zhang et al., 2022)
P-T of UHT granulite enclaves (2.3 Ma)(This study)
Depth (km)
Pressure (kbar)
Temperature (°C)